

Vortex Identification from Local Properties of the Vorticity Field

J.H. Elsas and L. Moriconi

*Instituto de Física, Universidade Federal do Rio de Janeiro,
C.P. 68528, 21945-970, Rio de Janeiro, RJ, Brazil*

A number of systematic procedures for the identification of vortices/coherent structures have been developed as a way to address their possible kinematical and dynamical roles in structural formulations of turbulence. It has been broadly acknowledged, however, that vortex detection algorithms, usually based on linear-algebraic properties of the velocity gradient tensor, are plagued with severe shortcomings and are also dependent on the choice of subjective threshold parameters in their implementations. In two-dimensions, a large class of standard vortex identification prescriptions turn out to be equivalent to the “swirling strength criterion” (λ_{ci} -criterion), which is critically revisited in this work. We classify the instances where the λ_{ci} -criterion blatantly fails and propose an alternative vortex detection scheme based on the local curvature properties of the vorticity graph (x, y, ω) – the “vorticity curvature criterion” (λ_ω -criterion) – which improves over the results obtained with the λ_{ci} -criterion in controlled Monte-Carlo tests. A particularly problematic issue, given its importance in wall-bounded flows, is the poor accuracy of the λ_{ci} -criterion for many-vortex configurations in the presence of shearing backgrounds. We show that the λ_ω -criterion is able to cope with these cases as well, if a subtraction of the mean velocity field background is performed, in the spirit of the Reynolds decomposition procedure. A realistic comparative study for vortex identification is then carried out for a direct numerical simulation (DNS) of a turbulent channel flow, including a three-dimensional extension of the λ_ω -criterion. In contrast to the λ_{ci} -criterion, the λ_ω -criterion indicates in a consistent way the existence of small scale isotropic turbulent fluctuations in the logarithmic layer, in consonance with long-standing assumptions commonly taken in turbulent boundary layer phenomenology.

PACS numbers: 47.27.-i, 47.27.De, 47.27.N-

I. INTRODUCTION

The twofold question on whether long-lived vorticity-carrying structures - coherent structures for short - can survive up to higher Reynolds numbers and play an important dynamical role in turbulence, with particular attention to the problems of isotropic and wall-bounded flows, has been for a long time a matter of great interest in the fluid dynamics community [1–7].

From a modeling perspective, the vorticity field $\vec{\omega}$ of incompressible flows (our focus in this work) can be considered to be a more fundamental observable than the velocity field \vec{v} , once the latter can be derived from the former as

$$v_i = -\epsilon_{ijk} \partial^{-2} \partial_j \omega_k, \quad (1.1)$$

where, above, ∂^{-2} stands for the Green’s function of the laplacian operator. Of course, Eq. (1.1) is nothing more than the Biot-Savart law in the fluid dynamical context.

One aims, in the so called “structural formulation of turbulence”, to achieve an expressive reduction in the number of degrees of freedom from the introduction of kinematical or dynamical models of coherent structures, the spatial support of strongly correlated vorticity lines. These special vorticity domains are then taken to be the sources of the turbulent velocity field, straightforwardly recovered with the help of Eq. (1.1). It is interesting to point out that while

structural modeling is still a very open problem, one finds, within the framework of wavelet compression techniques strong support for pursuing this direction of research [8–10].

Among the several types of turbulent flows, the turbulent boundary layer (TBL) is a particularly rich stage for the production and interaction of coherent structures [6], like streamwise and hair-pin vortices (often bunched in packets), the latter remarkably anticipated several decades ago by Theodorsen [11] and Townsend [12]. Due to the variable sizes of these structures, which are directly related to their distances from the wall, as depicted in the attached eddy hypothesis [12, 13], the TBL turns out to be a dynamical system characterized by strong multiscale couplings.

The pioneering structural approach of Perry and Chong [14] has underlined in many alternative ways subsequent investigations of the TBL along the years [15–20], devoted to the study of boundary layer phenomena like viscous drag, the existence of enhanced intermittent velocity fluctuations near the wall region and the crossover between turbulent kinetic energy production and dissipation, all of these being points of potential applied relevance. Nevertheless its appealing physical picture, the structural approach has been unable, so far, to address in a predictive way relevant phenomenological frameworks like the law of the wall or the broadly used k-epsilon turbulence models [21, 22].

A major problem in the structural formulation of

turbulence – paradoxically as it may sound – is the ambiguous meaning of the coherent structure concept itself. An operational answer to this question is to define a coherent structure as the compact flow configuration that is obtained, from numerical or experimental data, through the application of some postulated identification algorithm. Galilean invariant identification methods usually rely on the information encoded in velocity gradients, which tag regions of the flow characterized by “swirling motions” in locally co-moving reference frames.

Most of the discussions on structural aspects of turbulence adopt eulerian vortex detection methods like the Q-criterion [23–25], the Δ -criterion [26] and its closely related swirling strength criterion (λ_{ci} -criterion) [27, 28], or the λ_2 -criterion [29]. In all of these criteria, a scalar field, derived from the velocity gradient tensor, is used as a “marker” to indicate if a given point in the flow belongs or not to a vortex. Vortices, are therefore, identified as the connected regions mapped by such scalar fields.

Other classes of vortex identification methods are based on perhaps more involved mathematical formulations, like the proper orthogonal decomposition [30], neural network recognition algorithms [31], wavelet denoising theory [8], and the lagrangian approach [32].

Even though there are studies which have pointed out the shortcomings of the available vortex identification methods [28, 33–36], systematic investigations of their limitations are still in order. The most flagrant problems are the shape distortions of retrieved vortices and the subjective definition of threshold parameters, necessary to increase the efficiency of the identification algorithms. As we will emphasize in the following, a less obvious (but not less important) difficulty is associated with the effects produced on vortex identification by a shearing environment, as in free shear turbulence, turbulent boundary layers or channel flows.

The velocity gradient-based vortex identification strategies so far addressed in the literature are essentially equivalent, in two-dimensions, to the λ_{ci} -criterion. This is a key point in our discussion, which relies on a careful study of how the λ_{ci} -criterion performs for a variety of controlled “synthetic” two-dimensional flow configurations. It turns out that there are serious challenging difficulties with the use of the λ_{ci} -criterion, which have motivated us to introduce an alternative vortex identification prescription, referred to as the vorticity curvature criterion (λ_ω -criterion), a vortex identification method entirely based on local properties of the vorticity field.

Our results are centered on the analysis of two-dimensional coherent structures, which are important actors, for instance, in the dynamics of the atmosphere and the ocean [37], in purely two-dimensional turbulent systems [38], and also in the

properties of streamwise plane sections of turbulent boundary layer flows [39–43], which reveal the existence of spanwise vortex tubes. We introduce and study the problem of vortex identification for large ensembles of synthetic two-dimensional vortex systems and subsequently investigate, by means of a turbulent channel flow direct numerical simulation (DNS), the statistical features of boundary layer vortices from the point of view of both the λ_{ci} and the λ_ω criteria.

This work is organized as follows. To make the paper as self-contained as possible, we provide, in Sec. II, a detailed definition of the λ_{ci} -criterion, and classify, from the analysis of simple two-dimensional vortex configurations, its main issues. In order to overcome the observed difficulties with the λ_{ci} -criterion, an essentially threshold-free vortex identification method, the λ_ω -criterion, is proposed and discussed in Sec. III, which is found to considerably improve vortex detection for most of the problematic cases.

Monte-Carlo simulations of synthetic vortex systems are introduced in Sec. IV, as a way to evaluate how the λ_{ci} -criterion and the λ_ω -criterion automated algorithms perform for a large number of samples. We find, at this point, poor results for both vortex identification methods for the case of vortices in the presence of a strong background shear. To cope with that, we devise a background shear subtraction procedure, meaningful for statistically stationary flows, which points out the better, and reasonably good, performance of the λ_ω -criterion when compared to the one of the λ_{ci} -criterion.

We, then, move to the analysis of a more realistic scenario in Sec. V, provided by the numerical simulation of a turbulent channel flow. Having in mind all the issues discussed in the previous sections, it turns out that while the λ_{ci} -criterion fails to indicate isotropization of small scale turbulent fluctuations in the TBL logarithmic layer, the λ_ω -criterion can do so very successfully, which is a remarkable phenomenological result within the context of the structural formulation. We also discuss, in Sec. VI, the extension of the λ_ω -criterion to the case of fully three-dimensional flows, including some preliminary visualizations for the turbulent channel structures obtained in this way. Finally, in Sec. VII, we summarize our findings and point out directions of further research.

II. SWIRLING-STRENGTH ISSUES

The λ_{ci} -criterion for vortex identification relies on the analysis of the instantaneous topology of the velocity vector field [27]. In two dimensions (our main interest in this paper), one wants to single out points of the flow that can be classified either as sources or

sinks of streamlines. In more concrete terms, set as $(x_1, x_2) = (0, 0)$ the position of an arbitrary point in the flow, which has instantaneous vanishing velocity in the co-moving reference frame. Taking the velocity field to be “frozen”, we can write down the linearized equation of motion for a particle that follow the frozen streamlines of the flow in a neighborhood of the origin as

$$\dot{x}_i = A_{ij}x_j, \quad (2.1)$$

where $A_{ij} = \partial_j v_i|_{x=0}$ is the i, j matrix element of the velocity gradient tensor A . It is not difficult to show that spiraling orbits around the origin (the focus of motion) are necessarily associated with complex eigenvalues of A . The eigenvalue equation reads

$$\begin{aligned} \det(\partial_j v_i - \lambda \delta_{ij}) &= \\ &= \lambda^2 - \lambda \partial_i v_i + \det(\partial_j v_i) = 0. \end{aligned} \quad (2.2)$$

The “swirling strength” is the scalar field defined as the positive imaginary part of the complex eigenvalue $\lambda \equiv \lambda_{cr} + i\lambda_{ci}$. The λ_{ci} -criterion, thus, postulates that vortex domains are regions of the flow which have non-zero swirling strength. For incompressible two-dimensional flows, things are a bit simpler, once Eq. (2.2) tells us that these regions are the loci of points where the velocity gradient determinant is positive.

To exemplify the analysis, we illustrate how the λ_{ci} -criterion works for the prototypical Lamb-Oseen vortex [44], which is in fact an important building block in structural studies [18, 45, 46]. The Lamb-Oseen vortex is defined by the divergence free velocity field

$$v_i = \epsilon_{ij}x_j F(r), \quad (2.3)$$

where

$$F(r) = \frac{\Gamma}{2\pi r^2} \left(1 - e^{-\frac{r^2}{r_c^2}} \right). \quad (2.4)$$

Above, r_c and Γ denote the vortex core radius and its asymptotic circulation, respectively. The velocity gradient determinant can be easily derived as

$$\begin{aligned} \det(\partial_j v_i) &= F[F + rF'] = \left(\frac{\Gamma}{2\pi r^2} \right)^2 \times \\ &\times \left[1 - 2e^{-\frac{r^2}{r_c^2}} + e^{-\frac{2r^2}{r_c^2}} \left(3 - \frac{2r^2}{r_c^2} \right) \right] \end{aligned} \quad (2.5)$$

and it is shown in Fig. 1 as a function of r/r_c . The interesting point here is that the velocity gradient determinant is positive only within a finite distance $r \leq \bar{r}$ from the origin, so that the Lamb-Oseen vortex is identified as the disk on the density plot given in the inset of Fig. 1. From Eq. (2.5), we find that \bar{r} ,

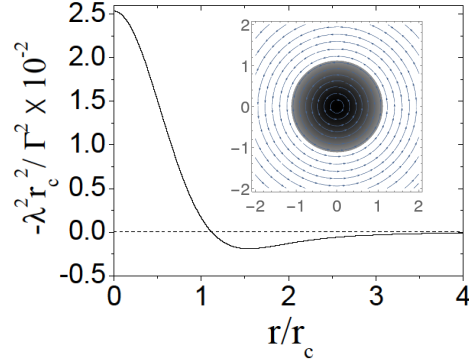


FIG. 1: The dimensionless velocity gradient determinant for the Lamb-Oseen vortex as a function of r/r_c . Inset: density plot of the swirling strength field and the vortex streamlines (coordinates are given in units of r_c).

and the vorticity flux across the disk, $\bar{\Gamma}$, are related to the corresponding vortex parameters as

$$r_c = \alpha \bar{r} \text{ and } \Gamma = \beta \bar{\Gamma}, \quad (2.6)$$

where, in terms of the Lambert W function [47],

$$\alpha \equiv \frac{1}{\sqrt{-\frac{1}{2} - W(-\frac{1}{2\sqrt{e}})}} \simeq 0.89 \quad (2.7)$$

and

$$\beta = \frac{1}{1 - e^{-\alpha^2}} \simeq 1.4. \quad (2.8)$$

It is common to assume, as a first approximation, that the connected regions highlighted by the λ_{ci} -criterion have, even in many-vortex two-dimensional systems, circular shapes, so that the relations given in (2.6) can be used to recover, in an automated fashion, the radius and the circulation parameters of the identified vortices. These same parameters can be obtained, alternatively, but with greater computational cost and comparable accuracy, from fittings, in the spotted regions, of the recorded velocity fields to the Lamb-Oseen pattern, Eqs. (2.3) and (2.4) [46].

Serious difficulties can arise in the implementation of the λ_{ci} -criterion when two or more vortices get close enough to each other, or if they are in the presence of a shearing background. However, there are no comprehensive works in the literature which attempt to define the conditions for the accurate use of this vortex identification method. Therefore, we put forward below, as a necessary stage for improvement over the λ_{ci} -criterion, an informal (and not exhaustive) classification of its important problematic issues for the case of two-vortex systems. To render our discussion free of ambiguities, whenever we refer to strict two dimensional vortices throughout the paper, we mean precisely Lamb-Oseen vortices.

(i) *Vortex Shape Distortion and Coalescence*

As it is shown in Fig. 2a, the shapes of two vortices get distorted as they approach each other, up to the point where they coalesce into a single vortex structure, as in Fig. 2b, due to the fact that the streamlines with opposite flow directions can mutually cancel in the region between them. Nevertheless the fact that there are two local swirling strength peaks in the merged region, it is not an obvious task how to disentangle them in practical automated analyses.

A way out to avoid the vortex merging problem would be to define a threshold parameter T and select regions of the flow which have $\lambda_{ci} > T$. This can actually break the coalesced structures back to two vortices again, but as a side effect other vortices in the system would be erased from detection. It is also likely that many other coalesced vortices in the flow would not be split in this way. Once there is not a clear prescription on how to define T , its choice is essentially subjective, and the threshold solution is far from being a well-established procedure. It should be clear, however, that there should be some room, in principle, for the implementation of iterative thresholding algorithms like the ones used in denoising theory [8].

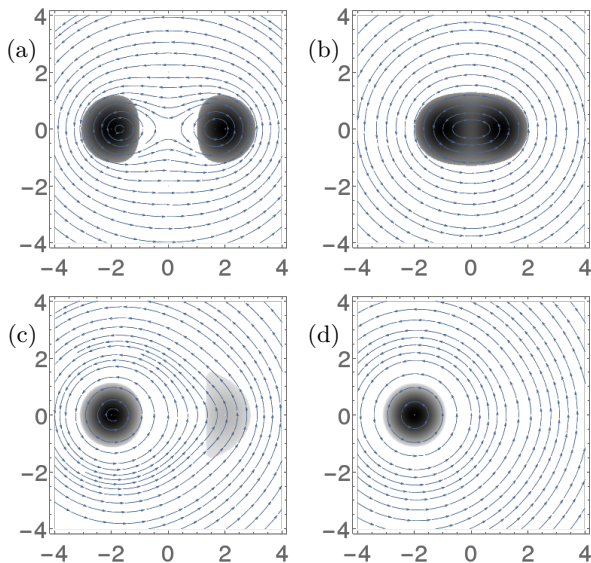


FIG. 2: In all of the four depicted cases, vortex pairs have the same core radius. Coordinates are given in units of r_c . Let Γ_L and Γ_R be the circulations of the left and right vortices, respectively. (a) Shape distortions of two near vortices with $\Gamma_L = \Gamma_R$; (b) vortex coalescence for a configuration with vortex centers separated by $2r_c$ and $\Gamma_L = \Gamma_R$; (c) configuration with vortex centers separated by $4r_c$ and $\Gamma_L = 5\Gamma_R$; (d) the same separation as in (c), but with $\Gamma_L = 10\Gamma_R$. The right vortex escapes detection by the λ_{ci} -criterion.

(ii) *Ghost Vortices*

Considering two vortices with the same radius, for instance, if one of them has larger circulation, shape distortion is, as expected, more pronounced for the vortex with smaller circulation. Instead of coalescence, however, the weaker vortex can disappear completely from the flow, if it happens to be close enough to the strong one. These situations are depicted in Figs. 2c and 2d.

(iii) *Spurious Vortices*

Spurious vortices can be misleadingly identified by the λ_{ci} -criterion in many-vortex configurations. These regions have, in general, relatively small area and circulation, making them, even if sometimes numerous, mostly non influential to the overall properties of flow, with the exception of counting statistics. Disregarding other aspects of Fig. 4b, the two vertically aligned and disconnected spots shown there are examples of spurious vortices generated from the approximation of two real vortices, further enlarged by the presence of background shear, identified in the picture as the two darker disconnected compact regions.

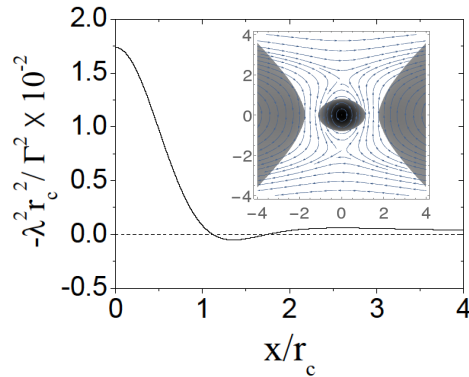


FIG. 3: The dimensionless velocity gradient determinant along the $y = 0$ axis, for a vortex of positive circulation Γ and radius r_c in the presence of a horizontal background shear of negative vorticity $\bar{\omega} = -0.05\Gamma/r_c^2$; Coordinates are given in units of r_c . Inset: density plot of the swirling strength field for this flow configuration.

(iv) *Background Shear Effects*

The most dramatic issues on the identification of vortices by means of the λ_{ci} -criterion are probably the ones associated to background shear effects, which for evident phenomenological reasons, are especially important in wall-bounded flows.

Take, as an illustrative example, the constant background shear with vorticity $\bar{\omega}$, described by the velocity field $(v_x, v_y) = (-\bar{\omega}y, 0)$, which can be superimposed to the velocity field produced by a vor-

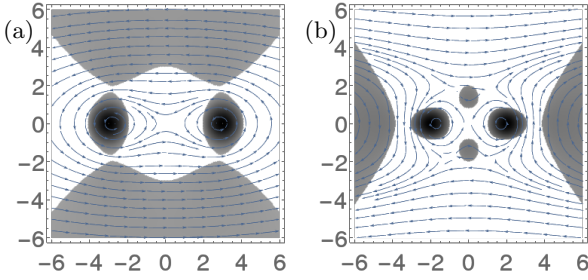


FIG. 4: The background shear is horizontal and both vortices have positive circulation Γ and radius r_c . Coordinates are given in units of r_c . The background vorticity is $|\bar{\omega}| = 0.05\Gamma/r_c^2$. (a) two vortices in a background shear of positive vorticity; (b) two vortices in a background shear of negative vorticity.

tex or a couple of vortices. Of course, the presence of background shear modifies the velocity gradient determinant. Analogously to Fig. 1, the velocity gradient determinant is plotted in Fig. 3 for $y = 0$, as a function of x/r_c . Differently from the free vortex case, the velocity gradient determinant becomes positive again at some distance from the origin, a fact that is related to the existence of two disconnected and spurious unbounded regions - henceforth referred to as “flaps” - which surround the real vortex, as shown in the inset of Fig. 3. Depending on the intensity and relative sign of the background vorticity, the vortex can disappear and only the flaps remain, or the flaps can coalesce with the vortex, forming a large, unbounded, structure.

In the test situation where we have two Lamb-Oseen vortices with identical circulations in the presence of a constant background shear, the flaps still show up, as can be seen in Fig. 4a and 4b. Furthermore, it turns out that if the background vorticity is opposite to the ones of the two vortices, then, besides the flaps, two spurious vortices appear. More complex patterns arise if additional vortices are superimposed to the background shear flow, once flaps and spurious vortices can also mutually interact.

The four general instances discussed above clearly indicate that the analysis of coherent structures through the use of the λ_{ci} -criterion, even though meaningful in cases where the vortex density and the vorticity of the background shear are small enough, can lead to inaccurate results, mainly in the investigation of turbulent flows, characterized by strong multiscale intermittent fluctuations of vorticity and strain. In the next section, we put forward an alternative vortex identification method, which has the local vorticity field as its main ingredient, and is devised to mitigate the alluded deficiencies of the λ_{ci} -criterion.

III. VORTICITY CURVATURE CRITERION

As a key point in understanding the pathological behavior of the λ_{ci} -criterion in many-vortex systems, it is useful to point out the connection between this criterion and the differential-geometric properties of the stream function $\psi = \psi(\vec{r})$. Note that in a dimensionless system of fluid dynamical units, the gaussian curvature K [48] of the stream function graph (x, y, ψ) can be written as

$$K = \frac{\partial_1^2 \psi \partial_2^2 \psi - (\partial_1 \partial_2 \psi)^2}{1 + (\partial_1 \psi)^2 + (\partial_2 \psi)^2} \quad (3.1)$$

$$= \frac{\partial_1 v_1 \partial_2 v_2 - \partial_1 v_2 \partial_2 v_1}{(1 + \bar{v}^2)^2} = \frac{\det(\partial_j v_i)}{(1 + \bar{v}^2)^2}. \quad (3.2)$$

It is clear, thus, from the comparison between (2.2) and (3.2), that in incompressible two-dimensional flows a point belongs to a vortex, according to the λ_{ci} -criterion, if and only if its stream function graph has positive gaussian curvature, like a dome.

For a typical vortex, which has a vorticity field $\omega(\vec{r})$ that decays faster than $1/r$, the streamfunction is asymptotically logarithmic, since

$$\begin{aligned} \psi(\vec{r}) &= -\partial^{-2} \omega(\vec{r}) \\ &= \frac{1}{2\pi} \int d^2 \vec{r}' \log \left(\frac{|\vec{r} - \vec{r}'|}{a} \right) \omega(\vec{r}'), \end{aligned} \quad (3.3)$$

where a is some (unimportant) arbitrary length scale in the flow. The Lamb-Oseen vortex, in particular, is associated to the stream function

$$\psi = \frac{\Gamma}{4\pi} [\log(r^2/r_c^2) - \text{Ei}(-r^2/r_c^2)], \quad (3.4)$$

where $\text{Ei}(\cdot)$ refers to the Exponential-Integral function [47], which is dominated, far from the origin, by the slowly varying logarithmic contribution in Eq. (3.4).

The asymptotic logarithmic profile of the vortex stream function implies that there are strong non-linear superposition effects that affect the curvature of the stream function graph associated to individual vortices in many-vortex systems. This is the main reason for all of the issues with the implementation of λ_{ci} -criterion, as discussed in the previous section.

The ideal set up to deal with vortex identification, thus, would be to base the analysis on the properties of spatially bounded fluid dynamic observables like the vorticity field carried by coherent structures. In two dimensions, the most immediate attempt along these lines would be to work with vorticity level curves, but this is a limited approach, since spurious vortices would proliferate and the subjective choice of thresholds would be unavoidable.

If we insist on vorticity as a fundamental element in a local vortex identification scheme, an interesting heuristic proposal is simply to replace the stream

function as it is used in the λ_{ci} -criterion by the vorticity field. Now, to find vortices we would look for positive curvature regions of the vorticity graph. This prescription is promising, but the inspection of some simple cases suggests that some refinement is still in order.

Consider, for example, four identical vortices which are placed at the vertices of a square. It is not difficult to show that the gaussian curvature of the vorticity graph is positive at the center of the square, even though there is no vortex there. Without loss of generality, if we take the real vortices to be “bumps” of the vorticity graph (i.e., if they have positive vorticity), then the spurious vortex at the center is a bowl, with idiosyncratic positive vorticity.

In more mathematical terms, we just mean that while $\omega\partial^2\omega$ is negative at the square vertices, it changes its sign at the center. This fact is the hint to establish a meaningful vortex identification prescription, the λ_ω -criterion, which relies on the local gaussian curvature properties of the vorticity graph. To introduce it in detail, we first define some notation. Taking the vorticity field $\omega(\vec{r})$, let

$$\tilde{v}_i(\vec{r}) = \epsilon_{ij}\partial_j\omega(\vec{r}) \quad (3.5)$$

and

$$\tilde{\omega}(\vec{r}) = -\partial^2\omega(\vec{r}) \quad (3.6)$$

be denoted, respectively, as the pseudo-velocity and the pseudo-vorticity fields. We can also write down the determinant of the pseudo-velocity gradient tensor as

$$\det(\partial_j\tilde{v}_i) \equiv -\tilde{\lambda}^2. \quad (3.7)$$

From the positive imaginary part of $\tilde{\lambda}$, consider the scalar field

$$\lambda_\omega \equiv \Theta(-\omega\partial^2\omega)\text{Im } \tilde{\lambda} = \Theta(\omega\tilde{\omega})\text{Im } \tilde{\lambda}, \quad (3.8)$$

where $\Theta(\omega\tilde{\omega})$ is the Heaviside filtering function that is expected to vanish for spurious vortices, like the one discussed in the preceding four-vortex example. Vortices are then identified by the λ_ω -criterion as the connected regions of the flow where $\lambda_\omega \neq 0$.

Comparing the λ_ω -criterion to the λ_{ci} -criterion, we note that the essential advantage of the former is that it depends locally on the vorticity field, which has sharp peaks and rapidly decaying tails for general vortices. The λ_{ci} -criterion, on its turn, is related to the curvature properties of the stream function graph, which has much broader peaks and tails, eventually leading to poor vortex identification resolution.

The λ_ω -criterion can be classified as a higher order derivative vortex identification scheme, since it depends on the evaluation of third order derivatives of the velocity field. Two decades ago this fact would

be probably a main objection to its practical use. However, taking into account the present status of optical measurement techniques such as particle image velocimetry and the fast increasing computational power of direct numerical simulations, there is an open avenue for the investigation of high-order derivative vortex identification methods. A point of great relevance here is that the λ_ω -criterion does not rely, as a matter of fundamental importance, on the use of subjective threshold parameters. This brings considerable simplification in the implementation of automated analyses of many-vortex configurations.

We re-examine, now under the light of the λ_ω -criterion, the relevant vortex identification issues presented in the previous section. The results are schematically depicted in in Fig. 5.

Without background shear, the λ_ω -criterion has, clearly, higher resolution than the standard λ_{ci} -criterion, since it is able to split coalesced vortices (Fig. 5b) that would otherwise be counted as one, and to recover ghost vortices (Fig. 5d). With constant background shear, we also find improvements: the vortex shape distortion is considerably reduced and the large, unbounded flaps are completely eliminated. However, as it can be seen in Fig. 5h there is a couple of relatively small λ_ω spurious regions in the form of vertical stripes, produced for the case where the two vortices have vorticity opposite to the one of the background. This undiserable effect is due to the specific form of the filtering function $\Theta(\omega\tilde{\omega})$. If a background with constant vorticity $\bar{\omega}$ is added to the vorticity field ω , the filtering function can be written as $\Theta((\omega + \bar{\omega})\tilde{\omega})$. Therefore, if $\bar{\omega}$ and ω have opposite signs and $|\bar{\omega}| > |\omega|$, the filtering function may, as a side effect, introduce errors or even hamper the identification of a true vortex. We will have more to say about this issue in Sec. IV.

In order to illustrate the crucial importance of the filtering function, and the general improvement gained with the λ_ω -criterion over the λ_{ci} -criterion, we show in Fig. 6 the analysis of a sample of 20 Lamb-Oseen vortices with varying radii and circulations, which are randomly distributed in a square domain. While the use of the λ_{ci} -criterion is unable to avoid the merging of two of the vortices and the disappearance of another one, all of the vortices are recovered with the use of λ_ω -criterion, which approximately preserves their original circular shapes.

If the filtering function were not used, many spurious regions would remain, as evidently pointed out in Fig. 6b. One notices that a few spurious vortices have survived the screening of the λ_ω criterion. We have to keep in mind, for proper applications of the λ_ω -criterion, that although leading to improvements, it is not free of errors, in the sense that probably any meaningful vortex identification method will eventually break in the analysis of extreme (hopefully unrealistic) flow conditions.

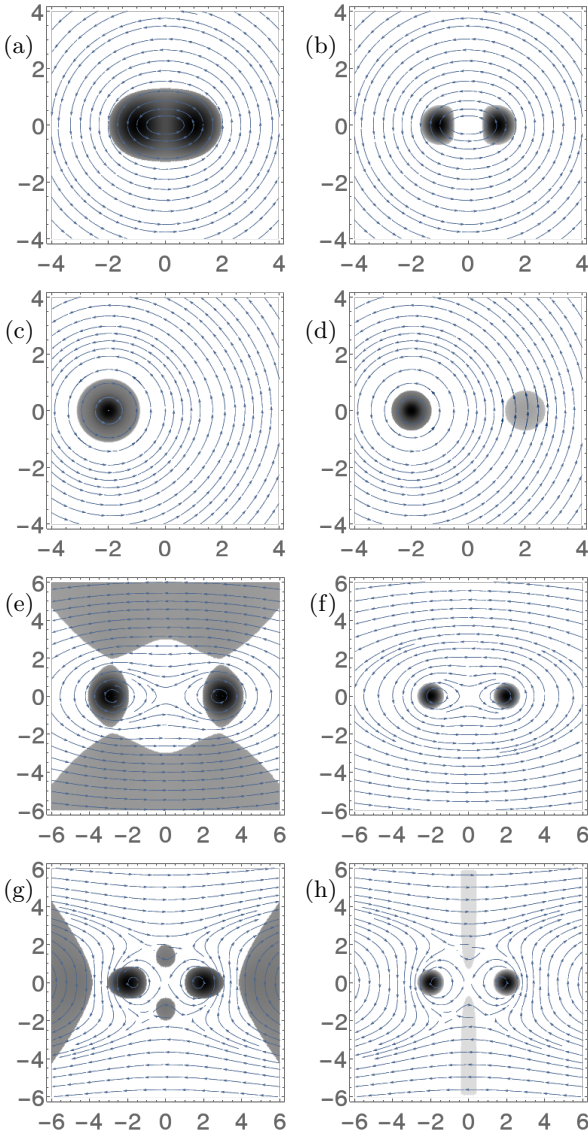


FIG. 5: The left column is a reproduction of the vortex configurations previously studied by means of the λ_{ci} -criterion in Figs. 2a, 2d, 4a and 4b. In the right column, the same configurations are reanalysed, now taking the λ_ω -criterion as the vortex detection tool.

So far, all of our arguments have been based on the inspection of a few representative analytical vortex configurations. Of course, more is needed to validate the λ_ω -criterion as a reliable tool. This is our next step, to be carried out with the help of extensive Monte Carlo simulations, where we consider, instead, discretized velocity derivatives for the analysis of large ensembles of synthetic many-vortex systems.

IV. MONTE-CARLO STUDY

To address a comparative study of accuracy for the λ_ω and the λ_{ci} criteria, we run Monte Carlo tests

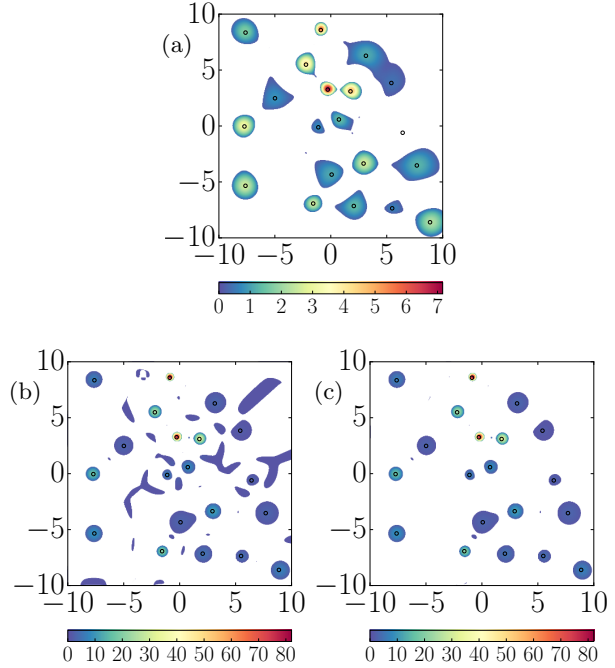


FIG. 6: Small open circles indicate the positions of 20 randomly distributed vortices. (a) vortex detection via the λ_{ci} -criterion. The phenomena of vortex coalescence and vortex erasing take place, respectively, in the first and fourth quadrants of the domain; (b) inaccurate vortex detection via the unfiltered λ_ω -criterion; (d) vortex detection via the filtered λ_ω -criterion, where all of the original vortices have been identified. Color online.

for large ensembles, where in each sample vortices are randomly distributed over the area of a square domain. The velocity field over a discretized grid is recorded and the two vortex identification criteria are applied to investigate how they perform in detecting and also in recovering the properties (circulation, radius, and position) of the original vortices.

In all of the synthetic samples, evaluations of the velocity gradient, pseudo-velocity and pseudo-velocity gradient have been done with five-point weighted finite differences, which in the worst situations (the ones involving three derivatives of the velocity field) have precision of $O(\delta^2)$ in the grid spacing δ . Integrations rely on bilinear interpolations, which are also precise to $O(\delta^2)$. The connected regions where vortices are detected are individualized in the grid with the use of a connected component labeling algorithm [49]. For each connected region R_k ($k = 1, 2, \dots$) we compute

$$A_k \equiv \pi \bar{r}^2 = \int_{R_k} d^2 \vec{r}, \quad (4.1)$$

$$\bar{\Gamma}_k = \int_{R_k} \omega(\vec{r}) d^2 \vec{r}, \quad (4.2)$$

$$\vec{r}_k = (x_k, y_k) \equiv \frac{\int_{R_k} \vec{r} \omega^2(\vec{r}) d^2 \vec{r}}{\int_{R_k} \omega^2(\vec{r}) d^2 \vec{r}}. \quad (4.3)$$

Eqs. (4.1) and (4.2) allow us to infer, respectively, with the help of Eq. (2.6), the real radius r_k and circulation Γ_k vortex parameters. While for the λ_{ci} -criterion α and β are already known from Eqs. (2.7) and (2.8), a similar and straightforward analysis for the λ_ω -criterion yields the analogous pair of parameters $(\alpha, \beta) = (\sqrt{2}, 1/(1 - 1/\sqrt{e})) \simeq (1.41, 2.54)$. Additionally, Eq. (4.3) gives the ‘‘center of enstrophy’’ coordinates for the position of the identified vortex.

We have worked, for a set of flow configurations of interest, with $N = 10^5$ Monte Carlo samples, each one containing $N_v = 20$ randomly distributed vortices, on a $[-9, 9]^2$ square (arbitrary length scale). The velocity field is exactly defined at the sites of a $N_x \times N_y = 200^2$ grid, which models the square box $[-10, 10]^2$. When sampled, vortex centers are always separated by distances greater than 1.2 times the sum of their radii [50]. Circulations and vortex radii are sampled with uniform random distribution in the domains given, respectively, by $1 \leq |\Gamma| \leq 20$ (or $-20 \leq \Gamma \leq -1$) and $0.5 \leq r_c \leq 1.5$.

Number of Samples	$N = 10^5$
Number of Vortices/Sample	$N_v = 20$
System’s Dimensions	$(L_x, L_y) = (20, 20)$
Vortex Positions	$-9 \leq x, y \leq 9$
Grid Size	200×200
Vortex Circulations	$\Gamma \in \pm[1, 20]$
Vortex Core Radii	$r_c \in [0.5, 1.5]$
Acceptance Cutoff	$\Gamma_0 = 0.5$
Vortex Pair Separation	$d_{ij} > 1.2 \times (r_{ci} + r_{cj})$

TABLE I: General definitions for the Monte Carlo simulations of the synthetic many-vortex two-dimensional systems.

As a way to get rid of spurious vortices, we furthermore prescribe that R_k is accepted as vortex only if $|\Gamma_k| \geq \Gamma_0$, for some small circulation scale Γ_0 . Note that this cutoff prescription is conceptually distinct from the imposition of a threshold, where the main worry is not exactly on the existence of spurious vortices as individual objects, but on specific - noise contaminated - regions of the flow. The circulation cutoff for vortex acceptance is defined as $\Gamma_0 = 0.5$. The Monte Carlo simulation definitions are summarized in Table I.

Motivated by the distribution of spanwise vortices observed in streamwise planes of turbulent boundary layers [39–42, 45, 46] we have considered, in our Monte Carlo simulations, five distinct flow patterns, denoted by latin capital letters from A to E, described in Table II.

To define the weak and strong shear regimes referred to in Table II, observe, as it can be derived from (2.2), that a vortex with peak vorticity ω_p dis-

appears from swirling strength detection if the vorticity of the background shear is $|\bar{\omega}| > |\omega_p|/2$, with $-\bar{\omega}\omega_p < 0$. Recalling that for a Lamb-Oseen vortex, $\omega_p = \Gamma/\pi r_c^2$, and that in our Monte Carlo samples, $|\Gamma| \leq 20$ and $|r_c - 1| \leq 0.5$, we take, as representative parameters, $\Gamma = 10$ and $r_c = 1$, which lead to $\omega_p/2 \simeq 1.6$. Weak and strong regimes are then defined as the ones which have background velocity fields given, respectively, by $(v_x, v_y) = (0.35y, 0)$ and $(v_x, v_y) = (1.6y, 0)$. Note that for flow patterns with either weak or strong background shear, the background vorticity is negative.

In the following, we organize the large lists of input and output vortex parameters (circulation, radius, and position) in the form of histograms that indicate how the λ_{ci} and λ_ω vortex identification criteria perform in the automated analysis of Monte Carlo ensembles.

Flow Pattern	Vortex Circulations	Background Shear
A	$1 \leq \Gamma \leq 20$	No Background
B	$1 \leq \Gamma \leq 20$	Weak
C	$1 \leq \Gamma \leq 20$	Strong
D	$-20 \leq \Gamma \leq -1$	No Background
E	$-20 \leq \Gamma \leq -1$	Strong

TABLE II: The five flow patterns considered in our Monte Carlo simulations.

Results for the flow pattern A are given in Fig. 7. The λ_ω -criterion has an excellent performance, while the λ_{ci} -criterion is mainly affected by vortex coalescence, which explains why the counting is reduced for the larger vortices, and why so many non-existent structures with circulation $|\Gamma| > 20$ have been artificially produced. One can note, from Figs. 7c and 7d that there are boundary effects in the distribution of vortices. This is actually due to the fact that by definition they ‘‘avoid each other’’ in the bounded domain. The same feature is observed in all of the other flow patterns.

For the flow patterns B and C, which have weak and strong background shear, respectively, the related histograms are given in Figs. 8 and 9. In the flow pattern B, as shown in Fig. 8, the λ_{ci} -criterion yields a small and uniform suppression of vortices in the samples, but the circulation and radius countings are actually close to the ones found for the flow pattern A. The λ_ω -criterion is still the better choice here, once it is able to capture the input vortices, but vortex counting is strongly affected by the addition of spurious vortices of small circulation and artificial structures like the stripes previously observed in Fig. 5h.

Driving our attention now to the flow pattern C, Fig. 9 tells us that both the λ_{ci} and the λ_ω criteria perform badly. It turns out that strong external shearing introduces, in general, relevant effects in

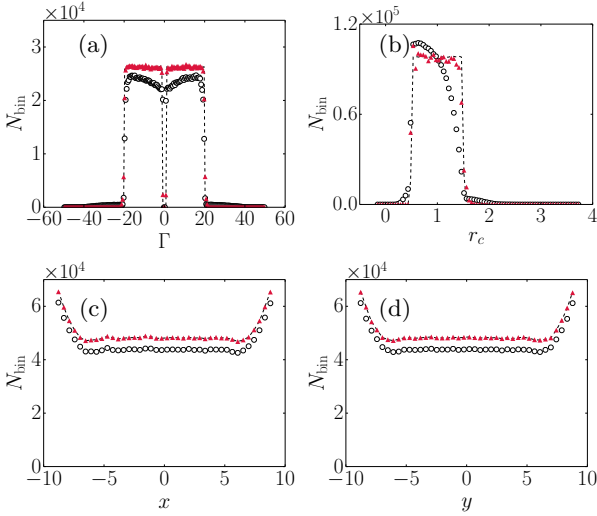


FIG. 7: Flow pattern A. Histograms for performance comparison between the λ_ω -criterion (triangles) and the λ_{ci} -criterion (circles), in the evaluation of vortex parameters. (a) circulations; (b) radii; (c) x coordinates; (d) y coordinates. The dashed lines are the histograms for the input data.

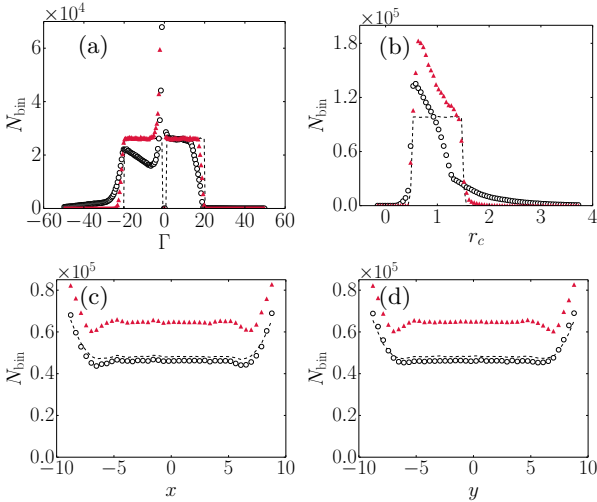


FIG. 8: Flow pattern B. All the rest as in the caption of Fig. 7.

vortex identification that demand improvement.

The visualization of a typical Monte Carlo sample of the flow pattern C is given in Fig. 10, where we see, as a dominant effect, coalescence percolation of flaps and vortices in the application of the λ_{ci} -criterion. On the other hand, the image associated to the λ_ω -criterion looks qualitatively different, and although most of the input vortices have been retrieved from the sample, they are surrounded by several spurious structures that can spoil histograms, like the ones we consider here.

In order to deal with the shortcomings associated with shearing/vorticity backgrounds, we put forward

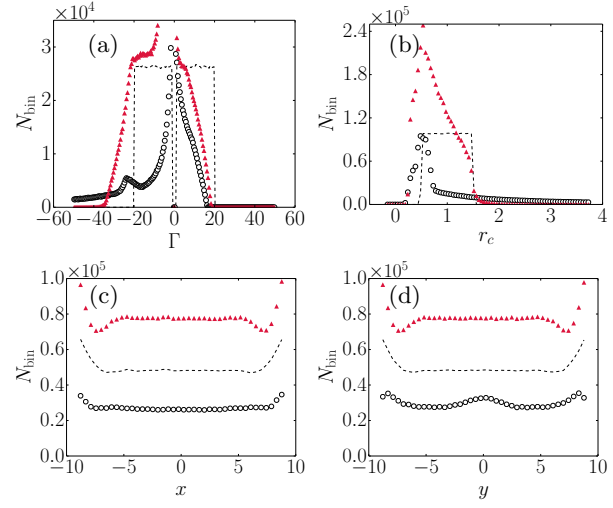


FIG. 9: Flow pattern C. All the rest as in the caption of Fig. 7.

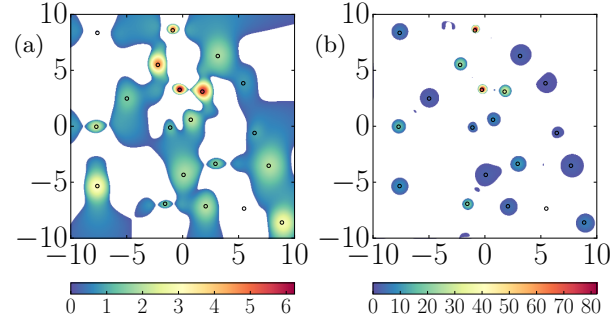


FIG. 10: A sample of 20 vortices - the same as in Fig. 6, now in the presence of strong background shear (flow pattern C), investigated through the (a) swirling strength and (b) the vorticity curvature fields. Color online.

an improved computational strategy, based on the subtraction of the background velocity field, sample by sample, from individual velocity field realizations. This is, of course, nothing more than the method of Reynolds decomposition. The idea is to revisit our previous analyses, by just replacing the original velocity field $v_i(\vec{r})$ by its fluctuations over the background, that is,

$$\delta v_i(\vec{r}) = v_i(\vec{r}) - \langle v_i(\vec{r}) \rangle, \quad (4.4)$$

where $\langle v_i(\vec{r}) \rangle$ stands for the expectation value of the velocity field taken over the ensemble of configurations. Furthermore, as an important point to avoid further spurious effects, we prescribe that a given point in the flow belongs to a vortex if it is detected in the vortex identification screening carried out with and without the background subtraction.

We compare, in the next six sets of histograms, the performance of the λ_{ci} and the λ_ω criteria, both with background subtraction procedure for the flow

patterns B and C, while analogous comparisons are done for the flow patterns D and E, with and without background subtraction. We do not report here the additional background subtraction analysis of the flow pattern A, since (as expected) we find that both criteria work again as in Fig. 7, due to the fact that the balanced mixing of vortices with positive and negative circulations produce a very small background.

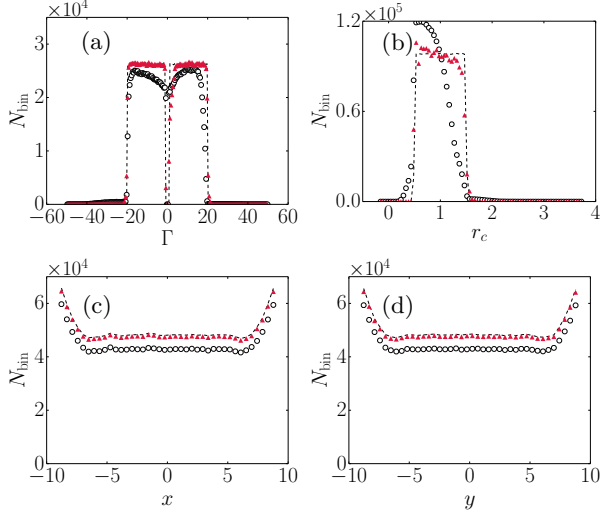


FIG. 11: Analysis of flow pattern B, with background subtraction. All the rest as in the caption of Fig. 7.

The weak shear case, flow pattern B, is given in Fig. 11, where both the λ_{ci} and λ_ω criteria are noted to improve in their performances, with a clear advantage for the latter.

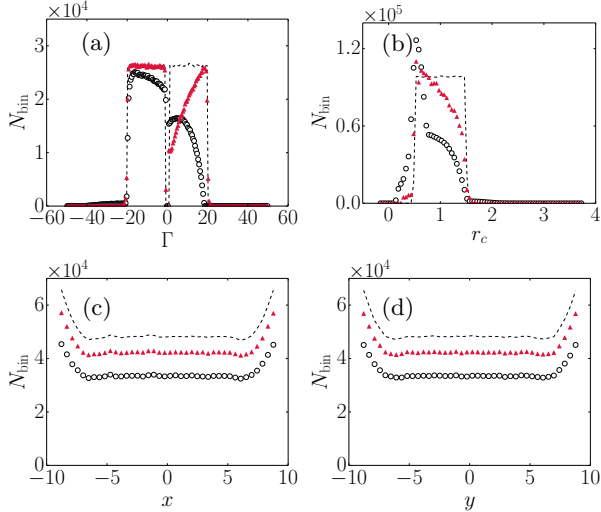


FIG. 12: Analysis of flow pattern C, with background subtraction. All the rest as in the caption of Fig. 7.

For the flow pattern C, we conclude, from Figs. 9 and 12, that the background subtraction proce-

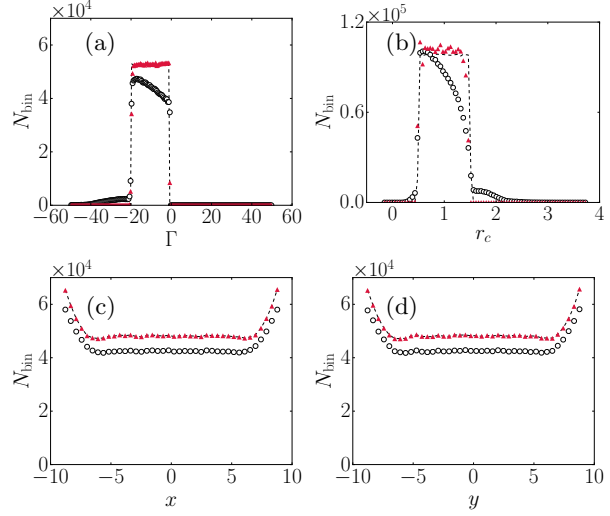


FIG. 13: Analysis of flow pattern D, without background subtraction. All the rest as in the caption of Fig. 7.

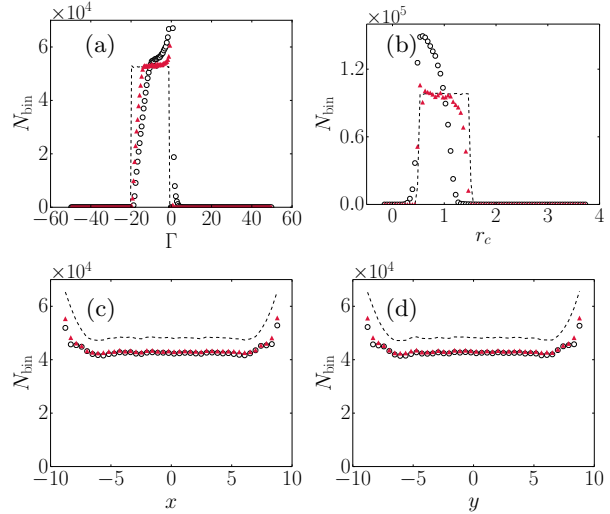


FIG. 14: Analysis of flow pattern D, with background subtraction. All the rest as in the caption of Fig. 7.

dure considerably improves the performance of the λ_ω -criterion, which now becomes valid as a method of vortex identification. Its only residual deficiency is the suppression of vortices which have relatively large radii and small positive circulations. This is, very clearly, a side effect of the Heaviside filtering function, which erases positive-circulation vortices that are completely “submerged” in the negative vorticity background.

As a way to loosely mimic some of the turbulence boundary layer characteristics found in streamwise layer characteristics found in streamwise planes, where the background vorticity has the same sign as most of the viscous layer vortices [41, 42, 46], we have devised the flow regimes D and E. Note that in the flow pattern D, there is no external background, $\bar{\omega} = 0$, but there is an essentially uni-

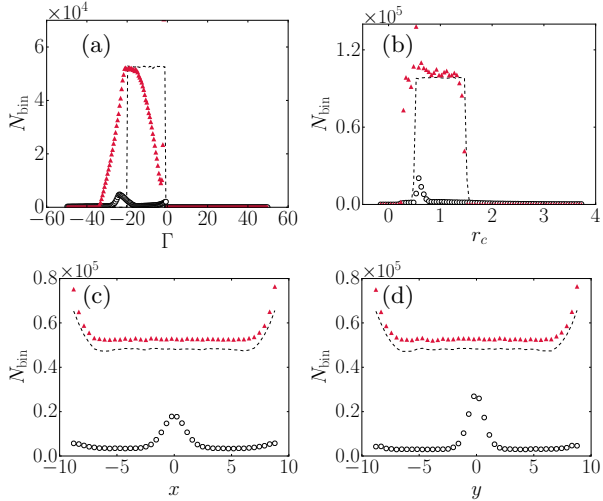


FIG. 15: Analysis of flow pattern E, without background subtraction. All the rest as in the caption of Fig. 7.

form negative vorticity background produced by the many-vortex system, because $\langle v_i(\vec{r}) \rangle \neq 0$. Curiously, as it can be seen from Figs. 13 and 14, the λ_ω -criterion is acceptable in both cases, but it works a bit better, for the flow pattern D, if the background were not subtracted. This has to do, this time, with the existence of vortices that are placed in regions of the flow where the local vorticity background is momentarily greater, due to the effect of fluctuations, than the mean self-induced vorticity background.

For the strong background case, flow pattern E, it turns out, as indicated from Figs. 15 and 16, that the background subtraction procedure leads to improvement, mainly in recovering circulation statistics, which brings the quality of vortex identification back to the reasonably good standards observed in the analysis of flow pattern D.

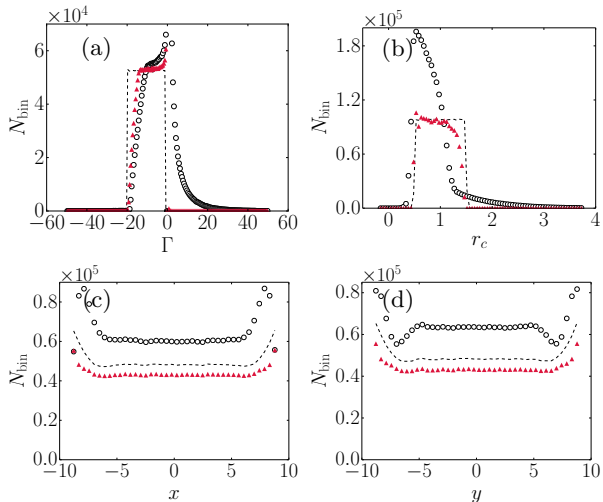


FIG. 16: Analysis of flow pattern E, with background subtraction. All the rest as in the caption of Fig. 7.

The above benchmarking Monte Carlo study shows that the λ_ω -criterion, enhanced by the background subtraction procedure, provides an appropriate identification prescription for the investigation of two-dimensional vortex systems. With the confidence acquired from the numerical experiments carried out with synthetic samples, we focus now on the analysis of a more realistic flow situation.

V. APPLICATION TO A TURBULENT CHANNEL FLOW

Cross sections of spanwise vortices, interpreted as heads of hairpin vortices, have been usually observed in streamwise plane sections of wall-bounded flows [39–43, 45, 46]. We have investigated the statistical properties of such two-dimensional vortex flow patterns by means of the λ_{ci} and the λ_ω criteria, for a turbulent channel flow DNS.

The turbulent channel flow simulation has friction Reynolds number $Re_\tau \simeq 395$ and setup parameters described in Table III. We follow here the simulation guidelines put forward by Kim, Moin and Moser [51]. The streamwise, normal to the wall, and spanwise coordinates are, respectively, x , y , and z ; periodic boundary conditions are imposed along the streamwise and spanwise directions; the grid is not uniform, with enhanced resolution near the walls, so that the viscous sublayer can be resolved with approximately one viscous length per lattice spacing. The simulation has been validated by standard tests, like the reproduction of the law of the wall and of statistical moments.

We have recorded, at every ten timesteps in the turbulent stationary regime, the projection of the velocity field of three parallel streamwise planes $z = 0$, $z = \pi/3$ and $z = 2\pi/3$. The ensemble defined in this way has a total number of 5268 flow configuration snapshots, which are, then, studied as two-dimensional velocity fields.

System's Dimensions	$(L_x, L_y, L_z) = (2\pi, 2, \pi)$
Grid Size	$256 \times 192 \times 192$
Kinematic Viscosity	$\nu \simeq 8.6 \times 10^{-4}$
Kinematic Pressure Gradient	$dP/dx = 0.11$
Simulation Time Step	$\Delta t = 1.2 \times 10^{-3}$

TABLE III: Parameters for the DNS of a turbulent channel flow.

We show, in Fig. 17, vortex identification images for one representative snapshot, analysed in three different ways. Figs. 17a and 17b give the results obtained from the application of the λ_{ci} -criterion without and with the use of the background subtraction procedure, respectively. Fig. 17c is the analogous result associated to the use of the λ_ω -criterion

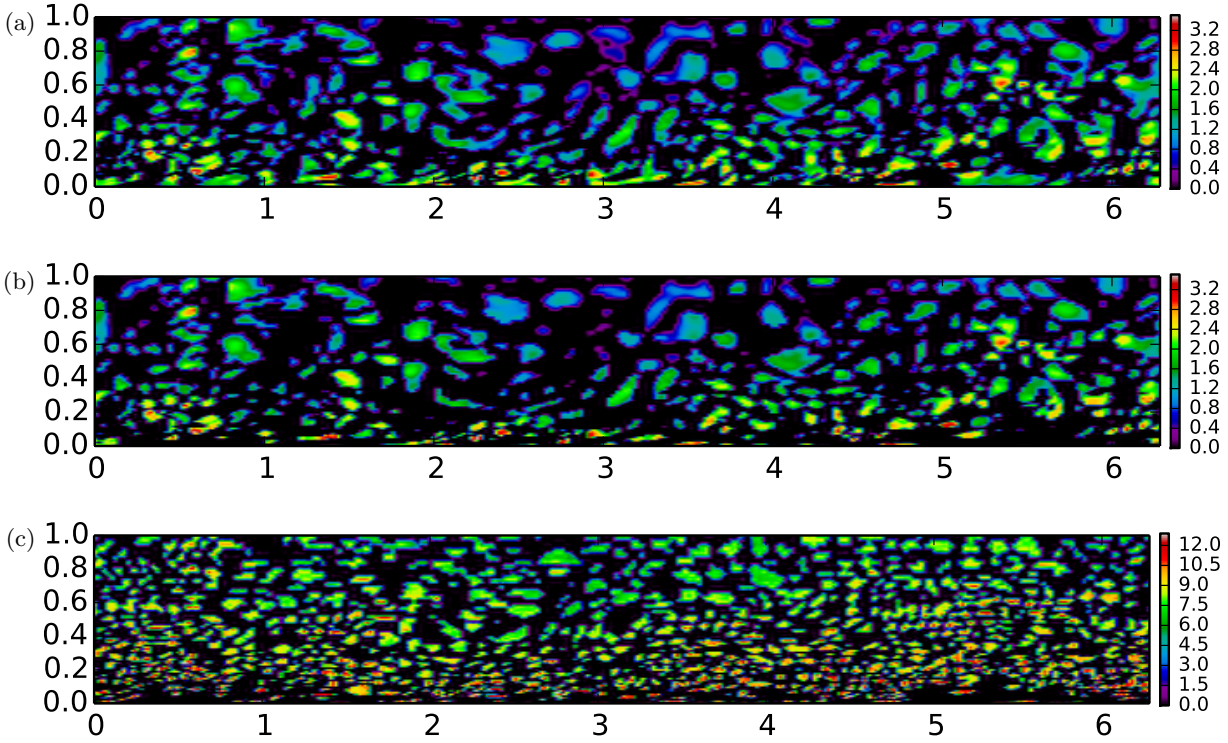


FIG. 17: Density plots of the λ_{ci} , [figures (a) and (b)] and the λ_ω [figure (c)] fields in a streamwise plane for the DNS of a turbulent channel flow, for all the channel extension and from the bottom wall up to the mid-channel height. No threshold is used in the vortex identification analyses. The background subtraction procedure is implemented only in figures (b) and (c). Color schemes are associated to linear and logarithmic scales, respectively, for the λ_{ci} and the λ_ω -criteria. Color online.

with background subtraction; no circulation cutoff has been used in the identification of vortices.

There are expressive qualitative differences between the two images produced by the λ_{ci} -criterion, for regions which are closer to the wall, where shear effects become more relevant. The λ_ω -criterion leads, on the other hand, to much better vortex resolution, but the background subtraction procedure does not lead, in visual terms, to expressive modifications - that's why we have not shown the picture associated to the application of the λ_ω -criterion without background subtraction. This, in fact, suggests that the flow takes place in weak background shear conditions. There are, however, small but meaningful improvements from the use of the background subtraction procedure that become evident only through histogram analysis, as we will show below.

As a practical remark to be emphasized here, we note that as it is a higher order derivative method, the λ_ω -criterion is related to identification fields that typically fluctuate over a much wider range of values than the ones associated to the λ_{ci} -criterion. This justifies our use of the logarithmic scale in the elaboration of the image given in 17c. Fixing attention on

the λ_ω -criterion, the natural application of the logarithmic scale implies, furthermore, that an optional use of thresholds is somewhat delicate for the case of turbulent (intermittent) flows: in fact, if the threshold is defined, for instance, as 20% of the maximum value of the logarithm of the λ_ω field, then its effects are likely to be irrelevant, since only structures with very low kinetic energy would be discarded; alternatively, if an analogous definition of the threshold is given in a linear scale, it is not difficult to see that almost all of the vortex structures would be erased in this way.

The streamwise plane snapshots of the turbulent channel flow are partitioned in thin streamwise stripes which have vertical width (bin size) $\Delta y^+ \approx 4$. Through a computational strategy analogous to the one discussed in the previous section, we identify vortices for each one of the stripes, and determine their mean circulation, peak vorticity, mean radius, and mean number as a function of the stripe distance to the wall. Results are reported in Figs. 18-21. We provide, for some of the pictures, insets which magnify their details, for the sake of better visual inspection.

Similar evaluations of the mean vorticity and mean

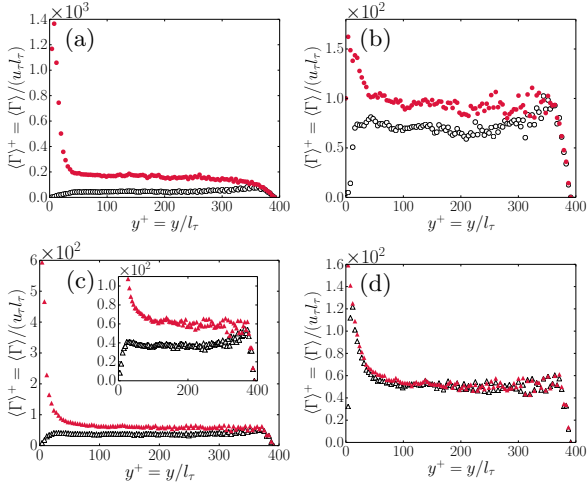


FIG. 18: Absolute mean values of the circulation for retrograde (open symbols) and prograde (solid symbols) vortices, as a function of the distance to the wall. All the quantities are given in wall units (friction velocity $u_\tau \simeq 0.34$ and viscous length $l_\tau \simeq 2.5 \times 10^{-3}$). Plots (a) and (b) are associated to vortex identification by the λ_{ci} -criterion, while (c) and (d) are associated to the λ_ω -criterion. The background subtraction procedure has been applied only for the results depicted in (b) and (d).

vortex radii as a function of the distance to the wall have been discussed in Ref. [46], where, however, vortex parameters are obtained from Levenberg-Marquardt fittings of the identified structures to the Lamb-Oseen vortex pattern. Their results, derived from a large turbulent database are compatible with ours, in the context of the λ_{ci} -criterion.

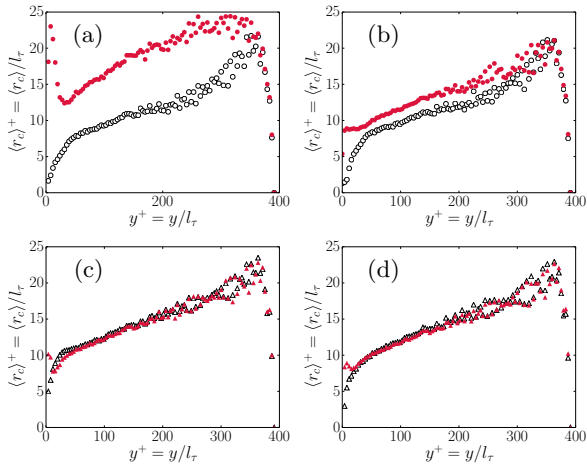


FIG. 19: Mean radius values for retrograde (open symbols) and prograde (solid symbols) vortices, as a function of the distance to the wall. All the rest as in the caption of Fig. 18.

The application of the λ_ω -criterion to the turbulent channel DNS data brings a phenomenologically interesting perspective on the statistical properties

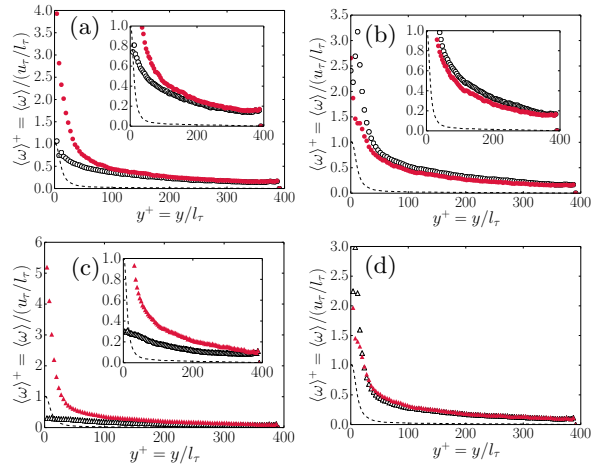


FIG. 20: Absolute mean values of the peak vorticity, i.e., $|\langle \Gamma / \pi r_c^2 \rangle|$ for retrograde (open symbols) and prograde (solid symbols) vortices, as a function of the distance to the wall. The dashed line is the average vorticity of the turbulent channel (which closely agrees with the law of the wall). All the rest as in the caption of Fig. 18.

of the spanwise vortices. It is clear, from Figs. 18 - 20, that even with the use of the background subtraction procedure, the λ_{ci} -criterion gives, for all the heights, distinct absolute values of the mean circulations, vorticities, and radii for the populations of positive (retrograde) and negative (prograde) vortices. The application of the background subtraction procedure in the λ_ω -criterion yields, on the other hand, a fine collapse of these quantities for $y^+ > 50$, which extends all throughout the logarithm boundary layer, as it can be appreciated from Figs. 18d, 19d, and 20d. If we now take a look at the populations of prograde and retrograde vortices in Figs. 21b and 21d, they are found to match each other in both criteria, but only after the background subtraction procedure is carried out.

We know, from the law of the wall, that the mean vorticity background is, in the logarithm layer, $\langle \omega^+ \rangle = 2.5/y^+$. It is clear, thus, from the inspection of Fig. 20, that the mean peak vorticity of the vortex structures is well above the vorticity background value for $y^+ > 50$, which tells us that there is in fact a weak background shear regime in the log-layer, following the convention put forward in the previous section. However, as it is suggested from Fig. 20d, the buffer layer is likely to be the region where shear effects can become relevant in the problem of vortex identification.

The data collapse attained in Figs. 18d, 19d, 20d, and 21d is an important point for the consolidation of the λ_ω -criterion, once it supports the long-standing phenomenological assumption of small scale turbulence isotropization in turbulent boundary layers [52–55]. The λ_{ci} -criterion yields data collapse only for the vortex counting histogram, Fig.

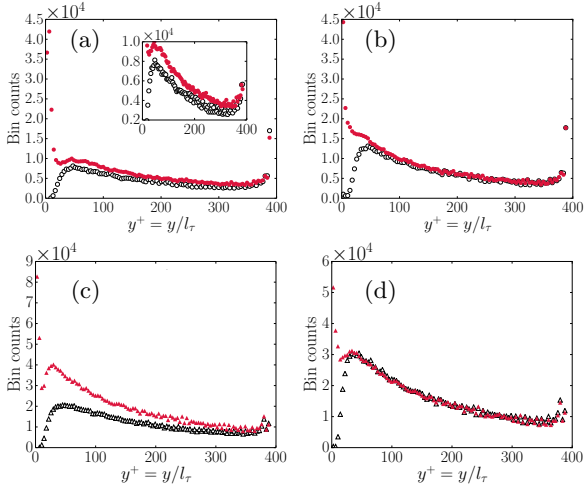


FIG. 21: Vortex counting per stripe of width $\Delta y^+ = 4$, for retrograde (open symbols) and prograde (solid symbols) vortices, as function of the distance to the wall. All the rest as in the caption of Fig. 18.

21b, failing to do so in the evaluations of vortex circulation, peak vorticity and radius parameters, as it can be clearly seen from Figs. 18b, 19b, and 20b.

The validity of the isotropic turbulence hypothesis in the turbulent boundary logarithm layer has been usually checked with the help of general theoretical relations that should hold for the expectation values of some local fluid dynamical observables [52–55]. This is a relevant aspect of the turbulent boundary layer phenomenology that has lacked so far proper corroboration within structural analyses, a fact due, essentially, to the limitations of the standard λ_{ci} vortex identification methodology.

VI. EXTENSION TO THREE-DIMENSIONAL VELOCITY FIELDS

It is interesting to devise three-dimensional generalizations of the λ_ω -criterion as a way to investigate the coherent structures that are behind their identified two-dimensional cross sections. There are several ways to do that, following two essential principles that all of the three-dimensional extensions have to satisfy. They have to

(i) be covariant under rotations

and

(ii) reduce to the λ_ω -criterion in two-dimensional slices of the flow.

With the above constraints in mind, let $\vec{\omega}(\vec{r})$ be the three-dimensional vorticity vector field, so that we can define, analogously to Eqs. (3.5) and (3.6), the pseudo-velocity and the pseudo-vorticity vector

fields, respectively, as

$$\tilde{v}_i(\vec{r}) = \epsilon_{ijk} \partial_j \omega_k(\vec{r}) \quad (6.1)$$

and

$$\tilde{\omega}_i(\vec{r}) = -\partial^2 \omega_i(\vec{r}) . \quad (6.2)$$

We can then pick up any of the standard three-dimensional vortex identification methods, like the Q or Δ criteria, to write down a straightforward generalization of the λ_ω -criterion. Taking the Q -criterion [23–25] as our specific example, recall that

$$Q(\partial_j v_i) = -\frac{1}{2} \partial_i v_j \partial_j v_i . \quad (6.3)$$

Vortex regions are defined as the connected sets of points where $Q > 0$. Resorting to the pseudo-velocity and pseudo-vorticity vector fields, the Q_ω -criterion, which extends the λ_ω -criterion to three dimensions, is defined from the scalar field

$$Q_\omega(\vec{r}) = \Theta(\omega_i \tilde{\omega}_i) Q(\partial_j \tilde{v}_i) . \quad (6.4)$$

In the same fashion as it is done with the Q -criterion, we look now for regions which have $Q_\omega > 0$ in order to find vortices. It is clear that as the Q -criterion reduces to the λ_{ci} -criterion in two-dimensions, an analogous result follows for the relation between the Q_ω and the λ_ω -criterion. Furthermore, the implementation of the background subtraction procedure can be readily done by the substitution of the velocity field by its fluctuation around the mean, exactly as given in the Reynolds decomposition prescription defined by Eq. (4.4).

In Fig. 22, we show how the Q and the Q_ω criteria perform for the simulation of the turbulent channel flow considered in Sec. V. As expected, there are many more, and better resolved, structures obtained from the use of the Q_ω -criterion. The color scale indicates the absolute value of the velocity field, which turns out to be a bit more intense for general regions of the flow in the case where the background subtraction procedure has been carried out.

We show, in these pictures, regions which have Q or Q_ω fields greater than prescribed thresholds, in order to obtain a clear visualization of flow structures at different distances from the wall. Figs. 22a and 22b are maps of coherent structures detected, approximately, for heights $y^+ < 50$, while Fig. 22c is related to structures found within $y^+ < 100$.

The Q_ω images, in contrast to the Q ones, suggest long-range correlations between regions which have higher magnitudes of the velocity field and the presence of vortex packets, a fact that can be related to the existence of the very large-scale motions (VLSMs) observed in boundary layer flows [56, 57].

Also, when we compare Figs. 22b and 22c, it is tempting to evoke here the conjecture that low speed

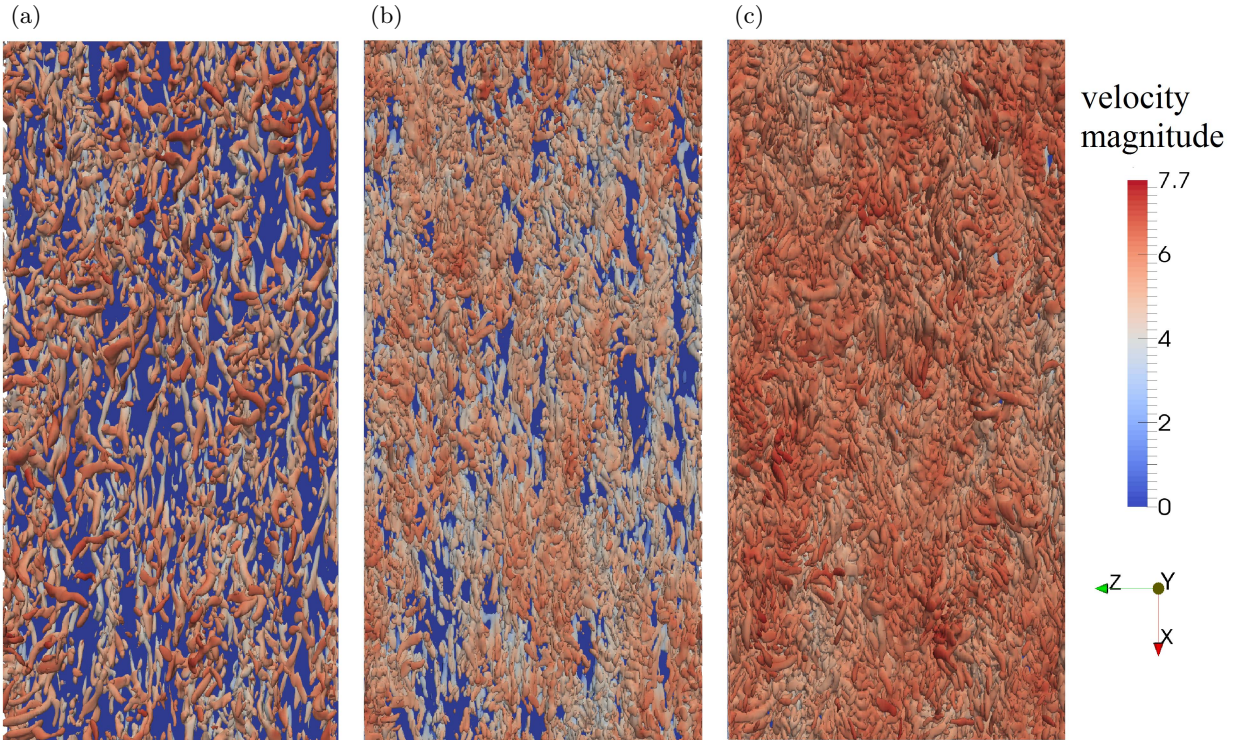


FIG. 22: Vortex identification for the turbulent channel flow DNS addressed in Sec. V. (a) Q -criterion with no background subtraction, $Q > 10^2$; (b) Q_ω -criterion with background subtraction, $Q_\omega > 1.1 \times 10^9$; (c) Q_ω -criterion with background subtraction, $Q_\omega > 1.2 \times 10^8$. Color online.

streaks are connected with the formation of aligned packets of hairpin vortices, as it has been put forward in Ref. [2].

The Q_ω -criterion seems, therefore, to be a promising tool to address the three-dimensional organization of vortex structures in boundary layers at high Reynolds numbers. However, since our aim in this section is just to give a first glimpse on three-dimensional vortex identification, we left this and other interesting issues to further comprehensive studies.

VII. CONCLUSIONS

We have introduced in this work an alternative vortex identification method – the λ_ω -criterion (or “vorticity curvature” criterion) –, which is fundamentally based on the local properties of the vorticity field. As the starting point of our approach, we have critically revisited the usual swirling strength, λ_{ci} -criterion, in order to classify its main shortcomings in simple two-dimensional vortex configurations. A careful and rigorous benchmarking analysis has then been carried out, through an extensive statistical Monte Carlo treatment of synthetic vortex systems, in order to compare the performances of the

λ_ω and the λ_{ci} criteria. We have been able to find, in this way, that the λ_ω -criterion leads, in general, to a considerably better and accurate identification of two-dimensional vortices, as well as of their parameters of circulation, size and position. We have also shown how to deal with possible spoiling external shear effects, by means of a simple background subtraction procedure, which amounts in the use of the local Reynolds decomposition of the velocity field.

We note that some further, but not very expressive, refinement of the λ_ω -criterion may be necessary for the cases of moderate/strong background shear in anisotropic vortex distributions (i.e., systems which have more negative than positive vortices, for instance), which may be relevant in flow conditions like the turbulent boundary viscous sublayer.

There are two crucial points for the observed good performance of the λ_ω -criterion: (i) the interesting local properties of the vorticity field, when compared to the ones of the streamfunction (which is a non-local function of vorticity), and (ii) the use of the filtering Heaviside function $\Theta(\omega\tilde{\omega})$ in the definition of the λ_ω -criterion, as given in Sec. III. This filter removes most of the spurious vortices and renders the method essentially free from the choice of subjective threshold parameters, an issue of serious concern in usual applications of the λ_{ci} -criterion.

We have provided evidence that the λ_ω -criterion can be successfully applied to the analysis of flow configurations obtained by direct numerical simulations, taking the paradigmatic turbulent channel flow as an example. It turns out that DNS velocity fields are smooth enough to allow the use of the λ_ω -criterion, a third order derivative scheme. We have been able, in this way, to address issues of isotropization in the turbulent boundary layer, which have, so far, eluded the structural approach. At variance with the λ_{ci} -criterion, the application of the λ_ω -criterion to the turbulent channel flow problem has led, for the first time (up to the authors knowledge), to a clear indication of isotropization in the turbulent boundary layer, within the structural point of view. More work is needed here, of course, in combination with the investigation of the three-dimensional coherent structures.

The λ_ω -criterion is directly generalizable to three-dimensions in more than one way. We have explored the three-dimensional extension motivated by the definition of the standard Q -criterion, which we have denoted as the “ Q_ω -criterion”. Preliminary visualizations based on the Q_ω -criterion show a profusion of well-resolved vortex structures, not revealed in any of the previous standard analyses based on the Q -criterion (plagued by both vortex coalescence and

erasing due to thresholding), and may shed light on the nature of the VLSMs, once they suggest some correlation between percolating stronger velocity fluctuations and the formation of vortex packets in the turbulent boundary layer. The study of other important boundary layer issues is in order, which can now be more accurately addressed. We mean, for instance, an investigation of coherent structures in the turbulent viscous layer, and their role in the production of viscous drag.

Acknowledgments

We would like to thank D. Dennis, R. Pereira, and J. Wallace for the many fruitful discussions during the course of this work. H. Anbarloei is specially acknowledged for his help with the numerical simulations of the turbulent channel flow discussed in this paper. The scientific atmosphere of the Núcleo Interdisciplinar de Dinâmica de Fluidos (NIDF) where part of this work has been developed has been a major source of motivation.

This work has been partially supported by CNPq (CT-CNPq/402059/2013-1) and FAPERJ.

-
- [1] S.K. Robinson, *Ann. Rev. Fluid Mech.* **23**, 601 (1991).
 - [2] R.J. Adrian, *Phys. Fluids* **19**, 041301 (2007).
 - [3] I. Marusic, B.J. McKeon, P.A. Monkewitz, H.M. Nagib, A.J. Smits, and K.R. Sreenivasan, *Phys. Fluids* **22**, 065103 (2010).
 - [4] J.M. Wallace, *J. Turbulence* **13**, 53 (2012).
 - [5] J. Jimenez, *Phys. Fluids* **25**, 101302 (2013).
 - [6] S. Tardu, *Coherent Structures in Wall Turbulence*, John Wiley & Sons (2014).
 - [7] D.J.C Dennis, *Ann. Braz. Acad. Sci.* **87**, 2 (2015).
 - [8] M. Farge, G. Pellegrino, and K. Schneider, *Phys. Rev. Lett.* **87**, 054501 (2001).
 - [9] G. Khujadze, R.N. van Yen, K. Schneider, M. Oberlack, and M. Farge, *Coherent vorticity extraction in turbulent boundary layers using orthogonal wavelets*, Proceedings of the Summer School Program, Center for Turbulence Research (2010).
 - [10] K. Yoshimatsu, T. Sakurai, K. Schneider, M. Farge, K. Morishita, and T. Ishihara, *Coherent Vorticity in Turbulent Channel Flow: A Wavelet Viewpoint*, in Proceedings of the International Symposium on Turbulence and Shear (2015).
 - [11] T.Theodorsen, *Mechanism of Turbulence* in Proceedings of the Midwestern Conference on Fluid Mechanics, Ohio State University, Columbus, OH, (1952).
 - [12] A.A. Townsend, *Coherent Structures in Wall Turbulence*, Cambridge University Press (1976).
 - [13] I. Marusic and R.J. Adrian, *Eddies and Scales of Wall Turbulence* in *Ten Chapters in Turbulence*, edited by P.A. Davidson, Y. Kaneda, and K.R. Sreenivasan, Cambridge University Press (2012).
 - [14] A.E. Perry and M.S. Chong, *J. Fluid Mech.* **119**, 173 (1982).
 - [15] A.E. Perry, S.M. Henbest and M.S. Chong, *J. Fluid Mech.* **165**, 163 (1986).
 - [16] K.R. Sreenivasan, *A Unified View of the Origin and Morphology of the Turbulent Boundary Layer Structure in Turbulence Management and Relaminarization*, edited by H.W. Liepmann and R. Narasimha, Springer-Verlag (1987).
 - [17] A.E. Perry and I. Marusic, *J. Fluid Mech.* **298**, 361 (1995).
 - [18] L. Moriconi, *Phys. Rev. E* **79**, 046306 (2009).
 - [19] I. Marusic, R. Mathis, and N. Hutchins, *Science* **329**, 193 (2010).
 - [20] R. Mathis, I. Marusic, S.I. Chernyshenko, and N. Hutchins, *J. Fluid Mech.* **715**, 163 (2013).
 - [21] H. Schlichting and K. Gerstein, *Boundary Layer Theory*, Springer-Verlag (2000).
 - [22] S.B. Pope, *Turbulent Flows*, Cambridge University Press (2000).
 - [23] A. Okubo, *Deep Sea Res. Ocean. Abs.* **17**, 455 (1970).
 - [24] J. Weiss, *Physica D* **48**, 273 (1991).
 - [25] J.C.R. Hunt, A.A. Wray, and P. Moin, *Eddies, Stream, and Convergence Zones in Turbulent Flows*, Center for Turbulence Research report CTR-S88, 193 (1988).

- [26] M.S. Chong, A.E. Perry, and B.J. Cantwell, *Phys. Fluids A* **2**, 765 (1990).
- [27] J. Zhou, R.J. Adrian, S. Balachandar, and T.M. Kendall, *J. Fluid Mech.* **387**, 353 (1999).
- [28] P. Chakabroroty, S. Balachandar, and R.J. Adrian, *J. Fluid Mech.* **535**, 189 (2005).
- [29] J. Jeong and F. Hussain, *J. Fluid Mech.* **289**, 69 (1995).
- [30] P. Holmes, J. Lumley, and G. Berkooz, *Turbulence, Coherent Structures, Dynamical Systems and Symmetry*, Cambridge University Press (1996).
- [31] J. Ferre-Gine, R. Rallo, A. Arenas, and F. Giralt, *Int. J. Neural Syst.* **7**, 559 (1996).
- [32] G. Haller, *J. Fluid Mech.* **525**, 1 (2005).
- [33] W. Schoppa and F. Hussain, *New Aspects of Vortex Dynamics Relevant to Coherent Structures in Turbulence in Eddy Structure Identification*, CISM Courses and Lectures No. 353, edited by J.P. Bonnet, Springer-Verlag (1996).
- [34] P. Chakabroroty, S. Balachandar, and R.J. Adrian, *J. Vis.* **10**, 137 (2007).
- [35] V. Kolář, *Int. J. Heat and Fluid Flow* **28**, 638 (2007).
- [36] Q. Chen, Q. Zhong, M. Qi, and X. Wang, *Phys. Fluids* **27**, 085101 (2015).
- [37] G.K. Vallis, *Atmospheric and Oceanic Dynamics*, Cambridge University Press (2006).
- [38] G. Boffetta, *Ann. Rev. Fluid Mech.* **44**, 427 (2012).
- [39] R.J. Adrian, C.D. Meinhart, and C.D. Tomkiss, *J. Fluid Mech.* **422**, 1 (2000).
- [40] R. Camussi and F. di Felice, *Phys. Fluids* **18**, 035108 (2006).
- [41] Y. Wu and K.T. Christensen, *J. Fluid Mech.* **568**, 55 (2006).
- [42] R.J. Adrian, *Phys. of Fluids* **19**, 041301 (2007).
- [43] D.J.C. Dennis and T.B. Nickels, *J. Fluid Mech.* **673**, 180 (2011).
- [44] G.K. Batchelor, *Introduction to Fluid Dynamics*, Cambridge University Press (2000).
- [45] J.A. LeHew, *Spatio-Temporal Analysis of the Turbulent Boundary Layer and an Investigation of the Effects of Periodic Disturbances*, PhD Thesis, Caltech (2012).
- [46] S. Herpin, S. Coudert, J.-M. Foucalt, J. Soria, and M. Stanislas, *Study of Vortical Structures in Turbulent Near-Wall Flows in Progress in Wall Turbulence: Understanding and Modeling*, edited by M. Stanislas, J. Jimenez, and I. Marusic, Springer (2011).
- [47] M. Abramowitz and I. Stegun, *Handbook of Mathematical Functions: with Formulas, Graphs, and Mathematical Tables*, Dover (1964).
- [48] W. Kühnel, *Differential Geometry: Curves - Surfaces - Manifolds*, American Mathematical Society (2006).
- [49] L. Shapiro and G. Stockman, *Computer Vision*, Prentice Hall (2001).
- [50] Eddy exclusion seems to be a realistic feature of boundary layer flows. See C.M. de Silva, J.D. Woodcock, N. Hutchins, and I. Marusic, *Phys. Rev. Fluids* **1**, 022401(R) (2016).
- [51] J. Kim, P. Moin, and R. Moser, *J. Fluid Mech.* **177**, 133 (1987).
- [52] S. Corrsin, *Local Isotropy in Turbulence Shear Flow*, Research Memo **58B11**, NACA (1958).
- [53] S.G. Saddoughi and S.V. Veeravalli, *J. Fluid Mech.* **268**, 333 (1994).
- [54] G. Xu, S. Rajagopalan, and R.A. Antonia, *Fluid Dyn. Res.* **26**, 1 (2000).
- [55] G. Gulitski, M. Kholmyansky, W. Kinzelbach, B. Luthi, A. Tsinober, and S. Yorish, *J. Fluid Mech.* **589**, 57 (2007).
- [56] K.C. Kim and R.J. Adrian, *Phys. Fluids* **11**, 417 (1999).
- [57] S.C.C. Bailey and A.J. Smits, *J. Fluid Mech.* **651**, 339 (2010).